In Situ Observation and Investigation of Mold Flux Crystallization by Using Double Hot Thermocouple Technology

LEJUN ZHOU, WANLIN WANG, DAOYUAN HUANG, JUAN WEI, and JIN LI

The crystallization processes of mold fluxes for casting low-carbon (LC) and medium-carbon (MC) steels were investigated by using double hot thermocouple technology (DHTT) in this article. The results showed that the glass phase was first formed at the cold side thermocouple (CH-2), when the LC mold flux (mold flux for casting low-carbon steel) was exposed to the temperature gradient of 1773 K (1500 °C) to 1073 K (800 °C); then, the fine crystals were precipitated at the liquid/glass interface and grew toward glass and later on to liquid phase. However, the crystals were directly formed at CH-2 when MC flux (mold flux for casting medium-carbon steel) was under the same thermal gradient. The growth rate of MC flux crystals was much faster than that of LC ones. Scanning electron microscope (SEM) and X-ray energy dispersive spectroscopy (EDS) analyses suggested that the crystals formed in LC mold flux were mainly dendritic cuspidine $Ca_4Si_2O_7F_2$, and the crystals formed from the liquid phase were larger than those from the glass. For MC mold flux, the earlier precipitated crystals were large dendritic $Ca_4Si_2O_7F_2$, whereas the later ones were composed of equiaxed $Ca_2Al_2SiO_7$ crystals. The results of DHTT measurements were consistent with the time-temperature-transformation (TTT) diagrams and X-ray diffraction (XRD) analysis.

DOI: 10.1007/s11663-012-9669-8

I. INTRODUCTION

MOLD flux is widely used in modern continuous casting of steel, and its main function can be divided into two categories: (1) protecting the steel from oxidation, insulating the steel from freezing and absorbing inclusions, when it floats on the top of liquid steel, and (2) lubricating the shell and moderating the heat transfer in the mold, when it infiltrates into the mold/shell channel. The crystallization of mold flux is regarded as one of the most important properties of mold flux, as it primarily controls the heat transfer and influences the lubrication of steel in continuous casting.[1,2] However, the actual situation in the mold cannot be observed directly because of the high temperature, transient fluid flow, complicated phase transition, chemical reaction *etc*. Thus, many kinds of technology were developed to study the crystallization behavior of mold flux. Through using the exothermic or endothermic property of the crystallization process, differential thermal analysis was adopted to investigate the crystallization behavior of mold flux.[3,4] Unfortunately, the low heating and cooling rate limited its application. The single hot thermocouple technology (SHTT) and double hot thermocouple technology (DHTT) were first developed by Kashiwaya *et al*.[5] for the *in situ* observation of mold flux crystallization, and these processes were favored by many other researchers[6–9] because of the visual as well as high heating and cooling rates. However, they were mainly used to construct the temperature-time-transformation (TT) and CCT diagrams of mold slag. A confocal scanning laser microscope was also used to study *in situ* the crystallization behavior of mold flux,[10,11] but it cannot obtain the desired temperature gradient that occurred in the mold. Furthermore, some other technologies were also tried to study the crystallization behavior of mold flux under conditions close to real mold, such as water-cooled probe technique,[12,13] infrared radiation emitter technique,[14] *etc*. However, they still have their own limitations.

In this article, the DHTT was used for the *in situ* observation of the crystallization processes of a typical low-carbon (LC) and medium-carbon (MC) mold fluxes under the simulated thermal conditions in the mold. One thermocouple was controlled at the temperature of 1773 K (1500 °C) to simulate the thermal condition of initial shell; the other thermocouple was set as 1073 K (800 °C), simulating the temperature of the solid mold flux layer next to the hot face of the copper mold wall. The distance between the two thermocouples was set as 2 mm, which corresponded to the width of mold/shell gap. The article provides a better understanding of the mold flux crystallization behavior in the real continuous casting mold, such as why the slag layer close to the mold wall was usually found to be glass when casting LC steels, while crystalline layer was formed in the solid slag when casting MC steels; and whether there was a difference between the crystals formed from glass and liquid.

LEJUN ZHOU, Ph.D. Student, WANLIN WANG, Professor, DAOYUAN HUANG, Postdoctor, and JUAN WEI and JIN LI, Graduate Students, are with the School of Metallurgical Science and Engineering, Central South University, Changsha 410083, P.R. China. Contact e-mail: Wanlin.Wang@gmail.com
Manuscript submitted November 24, 2011.
Article published online May 8, 2012.

II. EXPERIMENTAL

A. *Materials*

The compositions of the premelted mold fluxes for casting an industrial low- and medium-carbon steel were shown in Table I. They were prepared by melting regent-grade CaO, SiO_2, Al_2O_3, CaF, Na_2O, and Li_2O in an induction furnace at 1773 K (1500 °C) for 5 minutes to homogenize its chemical composition. After that, it was poured onto a cool steel plate to quench, and then it was subjected to crushing and grinding to make sample powders for the DHTT and SHTT measurements.

B. *Apparatus and Method*

The mold fluxes crystallization experiments were conducted using DHTT, and the TTT diagrams were constructed by using SHTT. The details of DHTT/SHTT apparatus have been described by Kashiwaya,[5] as shown in Figure 1.

Figure 2(a) was an illustration of double hot thermocouple technology, where a slag sample was mounted in between two B type thermocouples (CH-1 and CH-2), and a desired temperature gradient between the two thermocouples can be achieved through controlling the temperature of each thermocouple separately. Meanwhile, the images of mold flux crystallization were recorded by a charge-coupled device through the connected microscope for the observation and analysis. Because of the advantage of achieving a desired temperature gradient, the DHTT could be used to simulate the thermal conditions in the mold.

Figure 2(b) showed the schematic illustration of the SHTT, where the slag sample was mounted on one thermocouple and heated directly, while its temperature was recorded simultaneously.

For the DHTT experiments, the distance between the two thermocouples was set as 2 mm, according to previous reports.[15,16] The hot thermocouple (CH-1) was set as 1773 K (1500 °C) to simulate the shell surface temperature,[6,16] whereas the cold thermocouple (CH-2) was to simulate the solid mold flux interface temperature T_{INT}, which was between the solid mold flux and hot mold wall. Because of the solidification of liquid steel and mold flux, the air gap usually occurred between the hot side mold wall and mold flux; therefore, the T_{INT} was calculated through Eq. [1],[17,18] where the T_{HM} stands for the temperature of hot side of mold wall, q_T means the heat flux across the mold flux, and R_{INT} is the interfacial thermal resistance. The values for q_T, T_{HM}, and R_{INT} for the calculation were referred from previous studies and are listed in Table II. Consequently, the CH-2 (T_{INT}) was decided to be 1073 K (800 °C). The conditions for DHTT tests were shown in Figure 2.

$$T_{INT} = T_{HM} + q_T \times R_{INT} \quad [1]$$

When doing the DHTT experiments, the mold flux sample was first mounted on one of the two thermocouples; then, it was melted at 1773 K (1500 °C) with a rate of 15 °C/s. After eliminating bubbles and homogenizing its chemical composition for 180 seconds, the mold flux was stretched to 2 mm by the two thermocouples. Then, the temperature of CH-2 was quenched

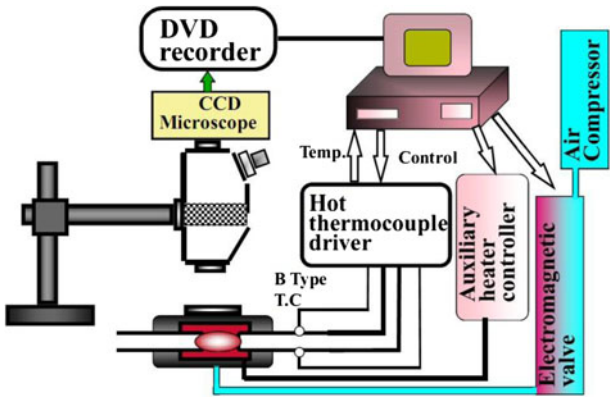

Fig. 1—The schematic of experimental apparatus.[5]

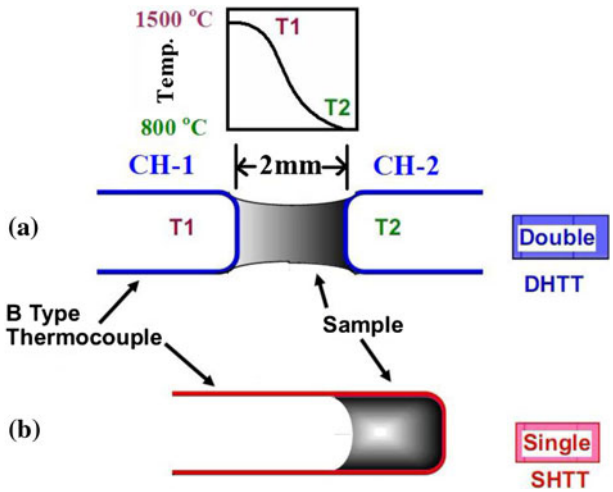

Fig. 2—The schematic of (*a*) double and (*b*) single hot thermocouples.[5]

Table I. Chemical Compositions of the Mold Fluxes after Premelting (in Mass Pct)

	CaO	SiO_2	Al_2O_3	MgO	F	Na_2O	Li_2O	CaO/SiO_2	Melting Point
LC	33.79	41.54	7.06	2.03	5.89	9.20	0.49	0.81	1390 K (1117 °C)
MC	43.51	32.86	12.08	2.02	3.92	5.11	0.50	1.32	1518 K (1245 °C)

Table II. Heat Flux, Mold Hot Face Temperature and Interfacial Resistance

Researchers	Ramirez-Lopez *et al.*[19,20]	Thomas and Coworkers[21,22]	Cho *et al.*[23,24]	This Study
q_T/MW/m^2	1.5 to 4.5	1 to 3	1 to 2	1.2
T_{HM}/K (°C)	≅473 (200)	473 (200) to 623 (350)		473 (200)
R_{INT}/(10^{-4}m^{2}K)/W	0.5 to 8	0 to 15	4 to 15	5

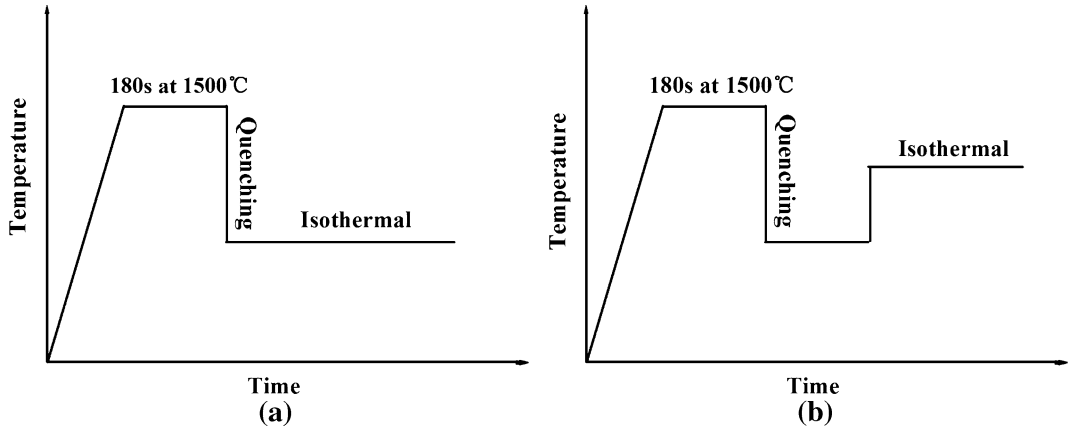

Fig. 3—Temperature controlling profile for TTT measurements: (*a*) crystallization from liquid and (*b*) crystallization from solid glassy phase.

directly to 1073 K (800 °C) to achieve the desired thermal gradient for the crystallization.

After DHTT experiments, the samples were then taken away and prepared for scanning electron microscope (SEM) and X-ray energy dispersive spectroscopy (EDS) analysis. To enhance the mold fluxes electric conductivity, the surfaces of samples were deposited with a thin layer of gold.

The TTT diagram construction was carried out in the following way: The sample powders were first heated in a single B type thermocouple at 1773 K (1500 °C) with the rate of 15 °C/s; and then, it was held for 180 seconds to eliminate bubbles and homogenize its chemical composition. After that, it was rapidly cooled down to different temperatures for isothermal crystallization (Figure 3(a)) when constructing the TTT diagrams of mold fluxes crystallization from liquid to crystal. Otherwise, it could also be quenched to the ambient temperature to form a glass phase; then, the glassy sample was heated to different temperatures for isothermal crystallization when constructing the TTT diagrams of mold flux crystallization from glass to crystal (Figure 3(b)).

To identify the phase composition of crystal mold flux, the X-ray diffraction was used. The X-ray diffraction (XRD) data were collected by using Cu Kα radiation (1.54184 Å), in a range of 2θ = 10 to 80 deg with a step size of 2 deg/s.

III. RESULTS AND DISCUSSION

A. *Evolution Process of LC and MC Mold Fluxes Crystallization under Simulated Thermal Conditions*

The temperatures history for the DHTT experiment of LC mold flux was shown in Figure 4, and eight

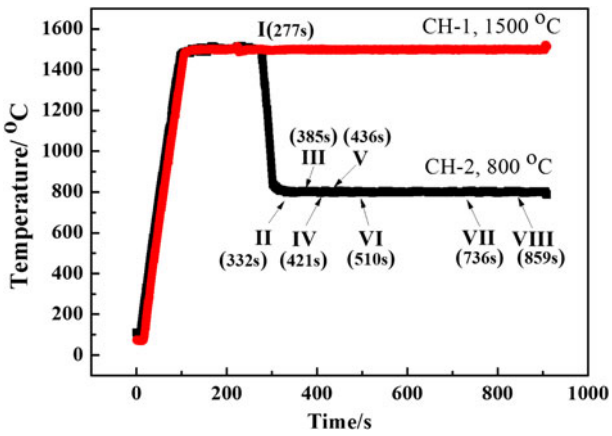

Fig. 4—Temperature history of DHTT for LC mold flux.

typical images standing for each stage were shown in Figure 5. The whole crystallization process lasted for approximately 495 seconds.

Figure 5(a) shows the state of mold flux was at position I (277 seconds) in Figure 4, where both thermocouples were at 1773 K (1500 °C). The mold flux was liquid and transparent as the temperature was above the melting point of the LC mold flux. Figure 5(b) was corresponding to the moment that the temperature of CH-2 was just reached 1073K (800 °C), at position II (332 seconds) in Figure 4, where the CH-2 thermocouple was darker. No crystal had precipitated, and the glassy phase was initially formed in the mold flux close to CH-2 because of the high cooling rate (30 °C/s), whereas the CH-1 side was still kept as liquid. When it stepped to position III in Figure 4, some very fine crystals (opaque area) were precipitated at the liquid/glass

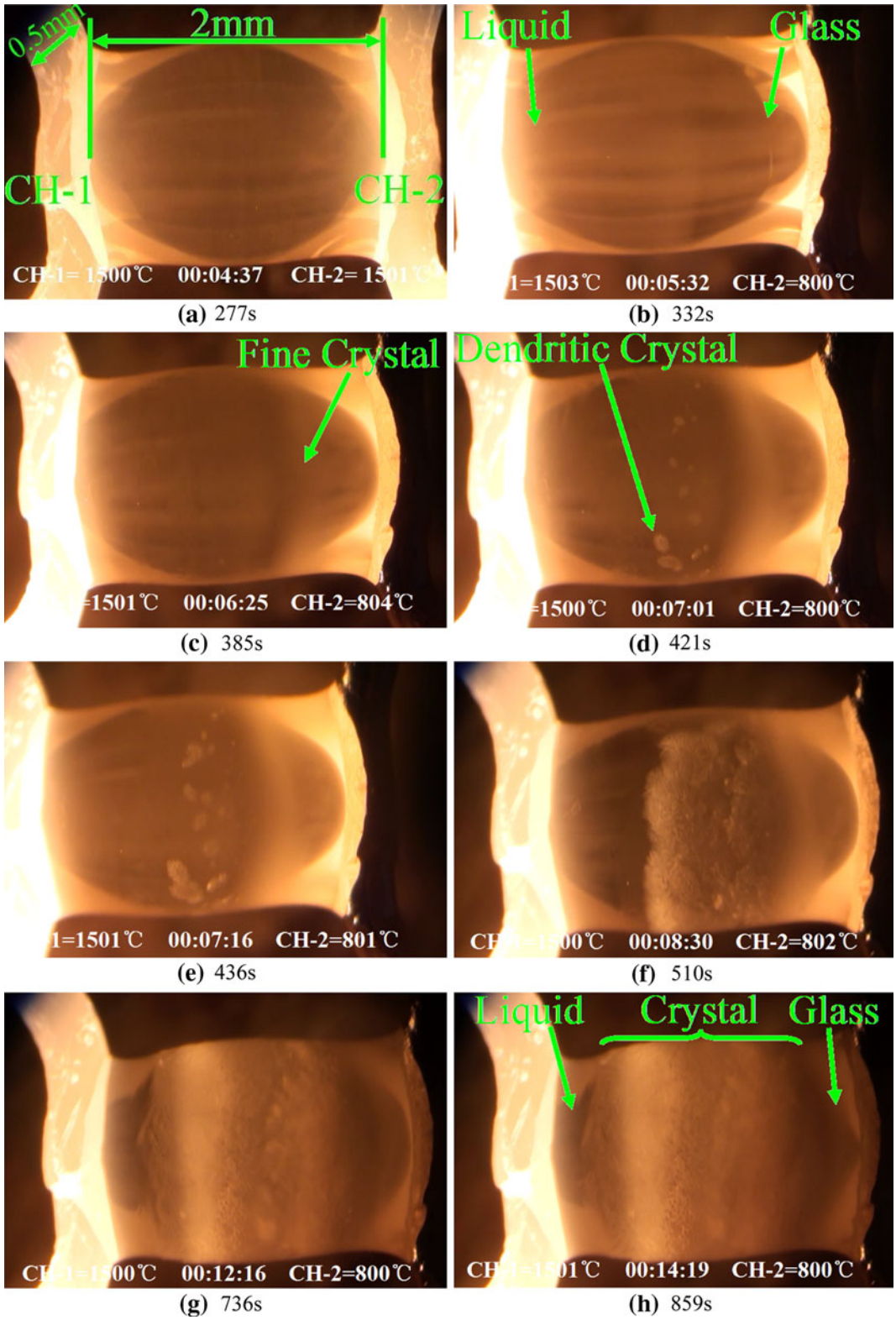

Fig. 5—Evolution process of LC mold flux crystallization.

interface and grew toward the glassy side (CH-2) as shown in Figure 5(c). When time went to 421 seconds, at position IV in Figure 4, some dendritic crystals were formed in the middle of liquid mold flux and grew toward CH-1 as shown in Figure 5(d). Figures 5(e) through (h) were the period of the crystallization development, corresponding to V-VIII in Figure 4, where the crystals were growing from the middle toward both sides of the thermocouples. In general, the crystals formed from the glassy phase toward CH-2 were finer

than those precipitated from liquid toward CH-1. Figure 5(h) was the moment that the structure of the whole mold flux stepped into a relative steady state. Apparently, there were still some transparent areas close to both CH-1 and CH-2, which stands for the liquid and glass layer of mold flux.

The variation of crystalline fraction of LC mold flux *vs* time was shown in Figure 6. The red dashed line was the moment that the temperature of CH-2 just reached to 1073K (800 °C) to simulate the moment that the liquid mold flux was infiltrated into shell/mold channel in the continuous casting mold. In two stages, the slope (the crystallization rate) was obviously greater than others. The first stage was from 365 seconds to 385 seconds, and the second stage was from 436 seconds to 510 seconds in Figure 6. The rapid increase of crystallization rate in the first stage was mainly caused by the initial crystallization from the glassy phase; the second stage was mainly caused by the later crystallization from the interface toward liquid and solid (Figures 5(e) and (f)), which may be because of the temperature distribution across the mold flux. As the temperature of CH-1 is 1773 K (1500 °C) and the temperature of CH-2 is 1073K (800 °C), there will be a continuous temperature distribution between CH-1 and CH-2, which indicates that the closer to the CH-1, the higher temperature the liquid mold flux will be; inversely, the close to the CH-2, the lower temperature of the glassy mold flux will be. For liquid mold flux, lower temperature is equivalent to higher undercooling, so the liquid mold flux at the liquid/solid interface with lower temperature will crystallize first, and then grows toward the CH-1. For glassy mold flux, a higher temperature is favorable for the transfer of ion clusters, so the glassy mold fluxes at the interface with a higher temperature will crystallize first, then toward CH-2.

Understanding of the mold flux crystallization in the mold is important, which gives a clear image of the mold flux thermodynamic behavior from the beginning when it is infiltrated into shell/mold channel to the moment it passes through meniscus and down to the bottom of the mold. At the bottom, the glass phase is initially formed close to the mold wall, then the crystals are developed at the liquid/glass interface and grow toward both liquid and glassy phases. Finally, the mold flux is kept a relatively steady state, *i.e.*, a liquid layer close to the shell, a glassy layer close to the mold, and the crystals developed in between them. It reflects the transient dynamic nature of the mold flux behavior that occurred in the mold, which in turn would affect the heat transfer and lubrication in the mold.

The temperature profile of the DHTT experiment for MC mold flux and some typical images corresponding to the crystallization process were also shown in Figures 7 and 8. It could be observed from Figure 7 that the whole crystallization process was lasted for approximately 49 seconds, which was much shorter than that of LC mold flux.

The crystallization process of MC mold flux could also be divided into several stages. Figure 8(a) was the moment that both thermocouples were at 1773 K (1500 °C), and the whole flux was kept as liquid, which was corresponding to the time of 264 seconds in

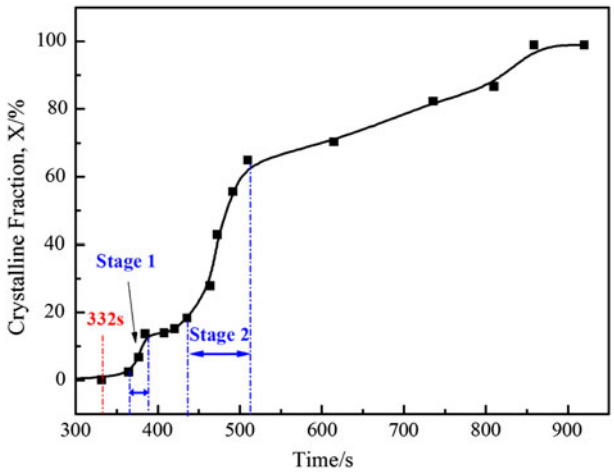

Fig. 6—The variation of crystalline fraction of LC mold flux *vs* time.

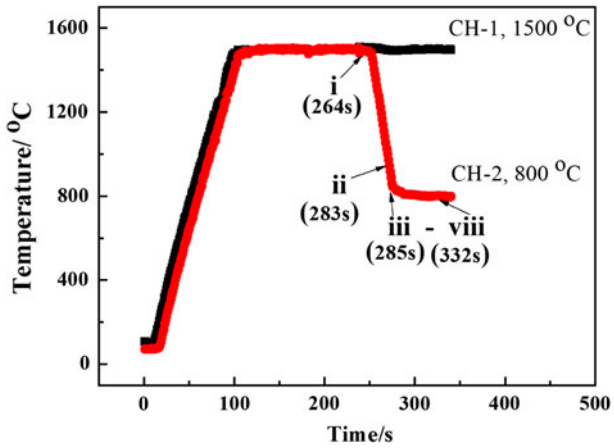

Fig. 7—Temperature history of DHTT for MC mold flux.

Figure 7. Unlike LC mold flux, the dendritic crystals were directly formed at the CH-2 side during the initial cooling of CH-2 as shown in Figure 8(b) corresponding to the position ii (283 seconds) in Figure 7. It suggested that the liquid MC mold flux was crystallized directly, and no glass phase formed during the cooling. Figures 8(c) through (h) represented the development of mold flux crystallization as shown from position iii to viii in Figure 7. It could be found that the crystalline layer mainly grew from the low temperature CH-2 to high temperature CH-1 at beginning. Later on, some crystals precipitated from the hot side (CH-1) and grew toward the middle (Figures 8(f) and (g)), which was described in detail in the SEM and EDS analysis. Meanwhile, Figure 8(f) showed crystals was breaking apart and moving toward the hot thermocouple. Normally, Marangoni flows developed from hot to cold because of the gradients in surface tension. In this experiment, the movement was internal, which suggested there was a strong surface flow from the hot thermocouple to the slag because of the surface tension gradients, as well as a return flow (for continuity) that accounted for the movement of the solid crystals from

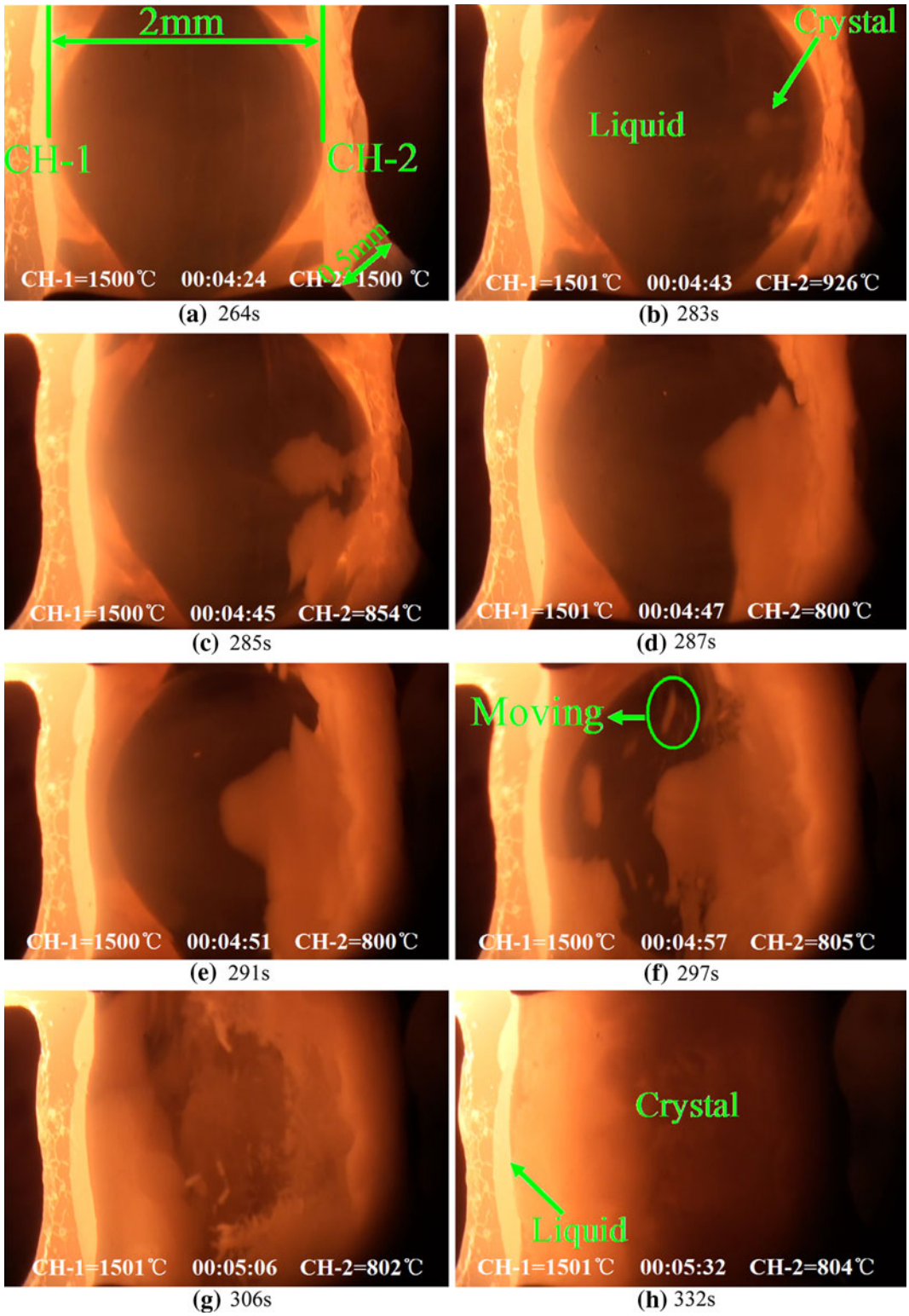

Fig. 8—Evolution process of MC mold flux crystallization.

the colder areas to the hotter areas. Those phenomena were also observed by Cramb and colleagues.[6,23–25] Figure 8(h) and position viii in Figure 7 was the moment that the crystallization was completed.

Figure 9 was the variation of crystalline fraction of MC mold flux *vs* time. The time that the mold flux started to crystallize was approximately 280 seconds. There was only one stage in the Figure 9 as all crystals were formed from the liquid phase. The basic trend of the curve in Figure 9 was that the crystalline fraction was increased slowly at the beginning; then, it jumped in the middle and turned down at the end.

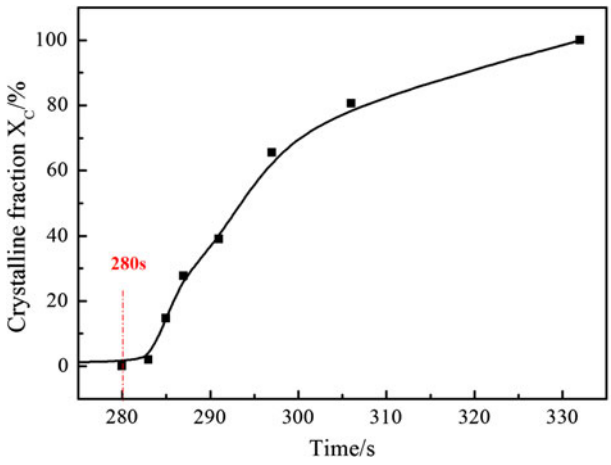

Fig. 9—The variation of crystalline fraction of MC mold flux *vs* time.

B. *SEM Analysis of the Crystal Morphologies Under Simulated Thermal Conditions*

The LC and MC mold fluxes were stripped from thermocouples for SEM and EDS analysis after DHTT experiments. Figure 10 was the result of SEM and EDS analysis of LC mold flux. Figure 10(a) was the general view of the mold flux, where the lower left side corresponds to the side of CH-2 (cool side) and the top right corner was the side of CH-1 (hot side) as shown in Figure 5. Four different phases appeared in the mold flux; they were glass 1 (originated from the rapid cooling of CH-2), crystal 1 (crystallized from glass in Figure 5(c)), crystal 2 (crystallized from liquid in Figure 5(d)), and glass 2 (formed from the remaining liquid when the experiment was stopped).

Figures 10(b) and (c) were the SEM photos and EDS results of crystal 1 and crystal 2, respectively. Compared with the SEM photos of crystal 1 with crystal 2, it is suggested that the morphologies of crystals formed from glass and liquid phase were different. Although both crystals were dendrites, apparently, the crystals formed from liquid were larger than those from glass. The results of EDS showed that the main elements of crystal 1 and crystal 2 were same as Ca, Si, O, and F, except the Au contamination of crystal 2. Their weight percentage were listed in tables in Figures 10(b) and (c). Au was found in crystal 2 as it was originated from the electric conductivity enhancing process as indicated in the experimental section. Both crystals were further analyzed through XRD in the next section.

The results of SEM and EDS analysis for MC mold flux were shown in Figure 11. Figure 11(a) was the general view of the MC mold flux after DHTT measurement, and there were only two kinds of crystals appearing in the flux. Figures 11(b) and (c) were the crystal morphologies and EDS results of the initial (from cold side) and later (from hot side) precipitated crystals during the crystallization of MC mold flux. The lower left quarter in Figure 11(a) was representing CH-2 side, whereas the top right corner was CH-1 side.

It could be found from Figure 11(b) that the earlier precipitated crystals (crystal 3) were large dendrites. And, the main elements of crystal 3 were Ca, Si, O, and F as listed in the table of Figure 11(b). However, Ca, Si, Al, and O were mainly appearing in the equiaxed crystal 4 as shown in Figure 11(c).

C. *TTT Diagram Construction of LC and MC Mold Flux Crystallization*

The TTT diagrams of LC mold flux crystallization from liquid and glassy phases were constructed as shown in Figures 12 and 13 separately. In the experiments, the 5 vol pct of crystallization was defined as the beginning of crystallization, and the 95 vol pct of crystallization was defined as the end of crystallization. It could be found from Figure 12 that the TTT curves of LC mold flux from liquid to crystal was single nose. The nose temperature was approximately 1273 K (1000 °C) and the incubation time of nasal tip (the position has the shortest incubation time) was approximately 227 seconds.

However, the isothermal crystallization trend from glass to crystal was changed because of the different nucleation and growth mechanism. The incubation time of nasal tip was reduced to 65 seconds at the temperature of 1273 K (1000 °C).

The TTT diagrams of LC mold flux crystallization both from liquid and glass phases could be used to explain the evolution process of LC mold flux crystallization as illustrated in Figure 5. As shown in Figure 12(a), the red cooling line with a rate of 30 °C/s does not intersect with the 5 pct of crystallization curve; thus, the glassy phase would be formed when CH-2 was cooled to 1073 K (800 °C) as occurred in Figure 5(b). It is consistent with the industry continuous casting of LC steels, where the glassy mold flux layer was always found on the side of the copper mold wall, which is a benefit to lubricating the mold and shell and enhancing the heat transfer in the mold.[26–28]

The TTT diagrams could also be used to explain why the crystal particles were first precipitated at the interface of glass/liquid and grew toward the glassy phase first, then precipitated in liquid as shown in Figures 5(c) and (d). According to the combination of the 5 pct of crystallization TTT diagrams in Figure 14(a), the incubation time of LC mold flux crystallization from glass was much shorter, especially around the nose temperature (1223 K to 1323 K [950 °C to 1050 °C]) than that of from liquid; in addition, the liquid/glass interface temperature was estimated at approximately 1273 K (1000 °C), nose temperature, according to the temperature gradient between the two thermocouples. Therefore, the crystallization was first initiated in the solid glass around the interface and grew toward to the glass.

The crystals formed from liquid and glass phases were further identified by X-ray diffraction (Figures 12(b) and 13(b)). Only cuspidine ($Ca_4Si_2O_7F_2$) was found in those samples. This result confirmed the results of EDS analysis in Figure 10 that both crystal 1 and crystal 2 were $Ca_4Si_2O_7F_2$.

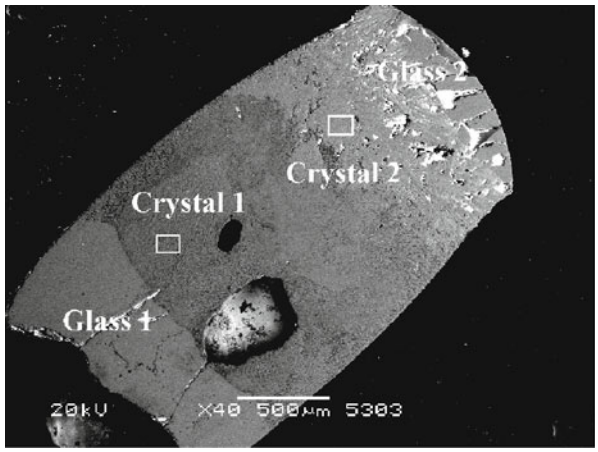

(a)

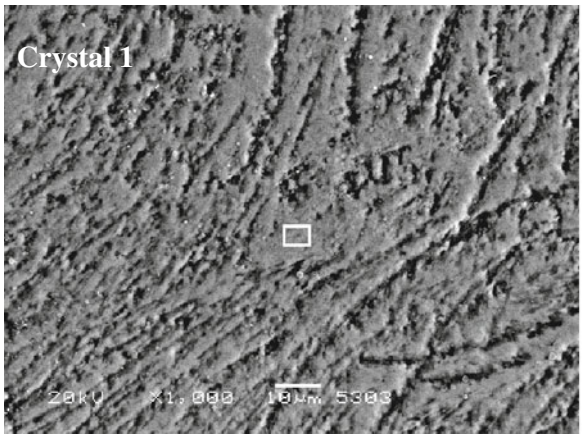

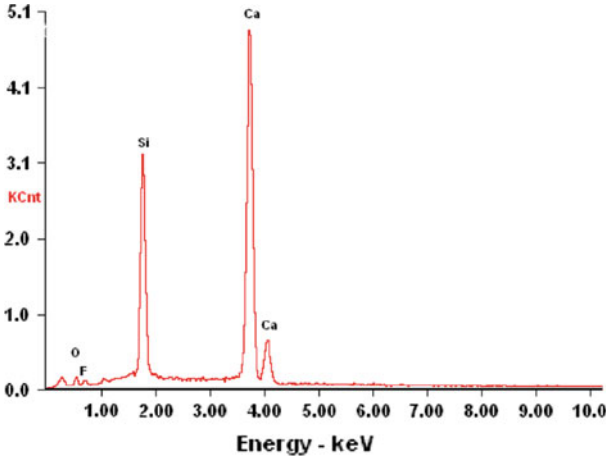

Element	Ca	Si	O	F
Wt%	57.29	22.22	14.7	5.16

(b)

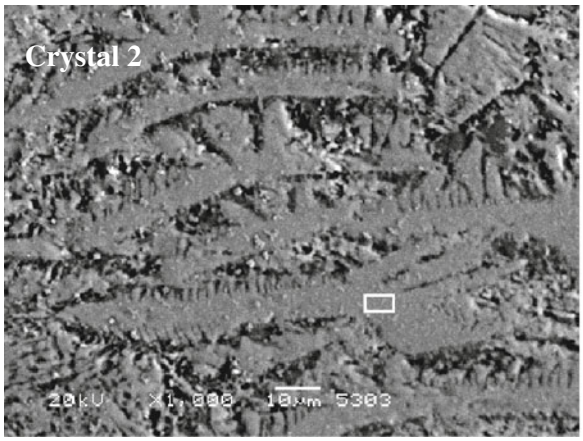

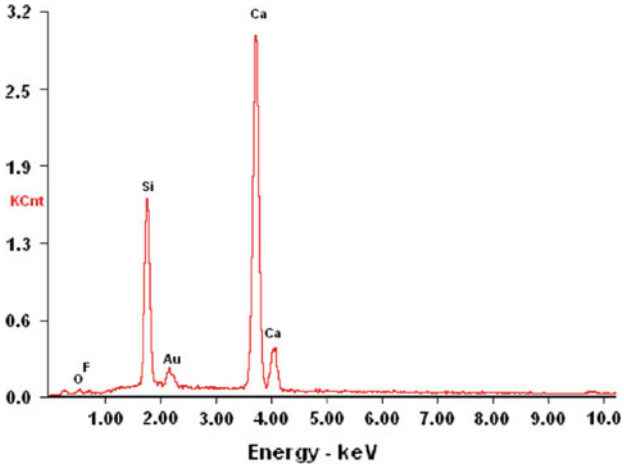

Element	Ca	Si	O	F	Au
Wt%	52.21	22.70	8.46	4.40	12.23

(c)

Fig. 10—SEM and EDS of LC mold flux: (*a*) general view, (*b*) crystal 1, and (*c*) crystal 2.

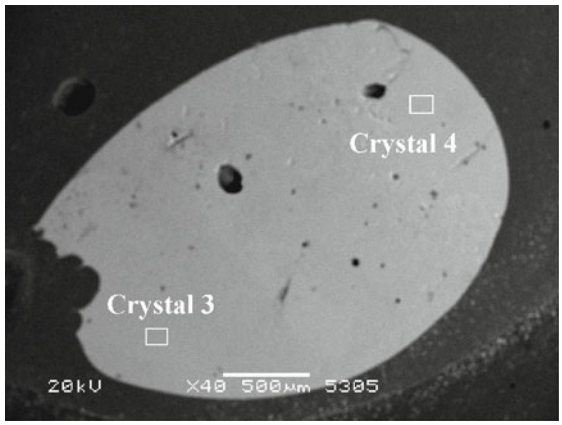

(a)

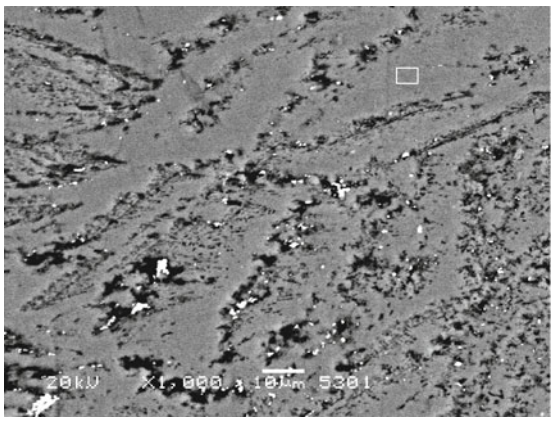

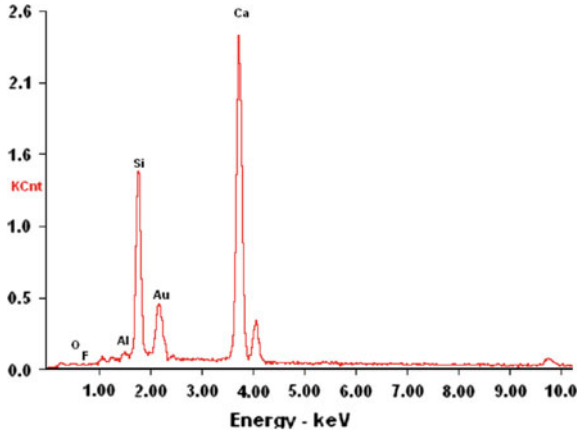

Element	Ca	Si	O	F	Al	Au
Wt%	47.42	19.4	10.26	4.79	2.01	16.12

(b)

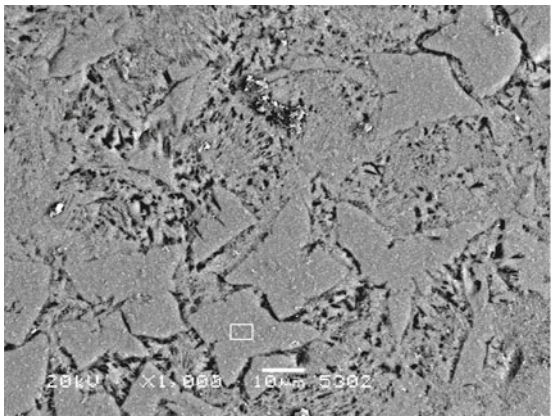

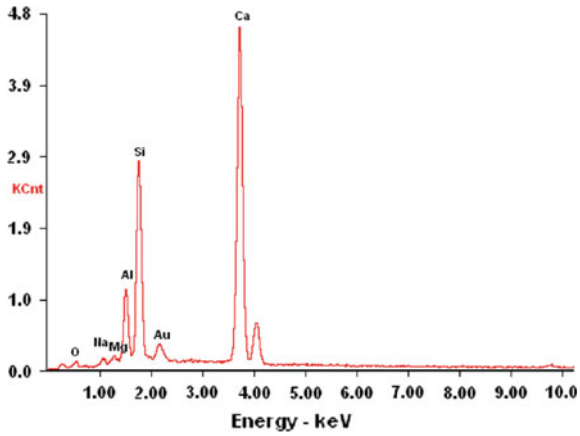

Element	Ca	Si	O	Al	Mg	Na	Au
Wt%	49.37	15.63	7.72	14.63	2.96	1.57	8.12

(c)

Fig. 11—SEM and EDS of MC mold flux: (*a*) general view, (*b*) crystal 3, and (*c*) crystal 4.

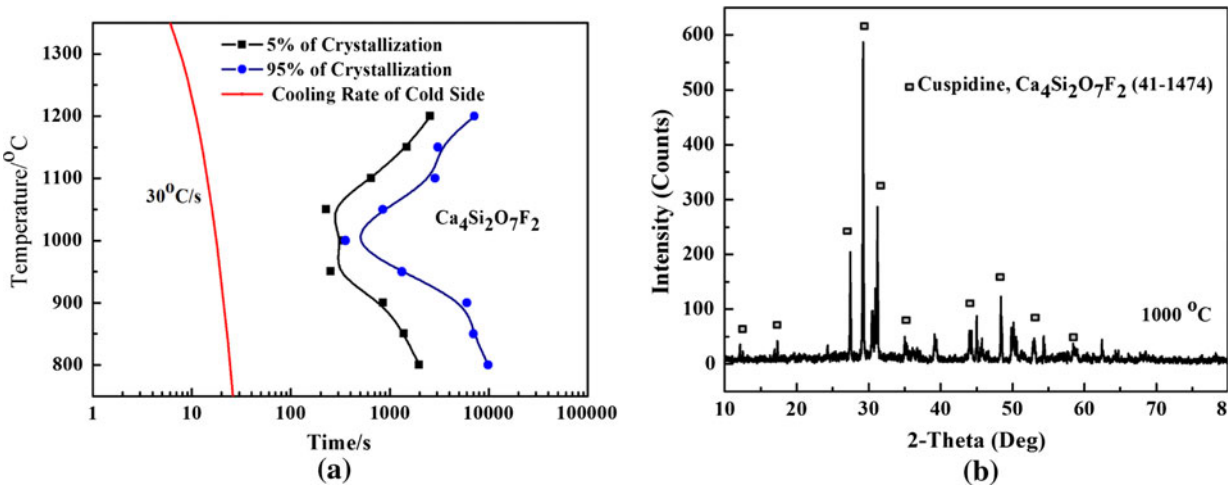

Fig. 12—TTT diagram of LC mold flux from liquid to crystal: (*a*) TTT diagram and (*b*) XRD of crystal at 1273 K (1000 °C).

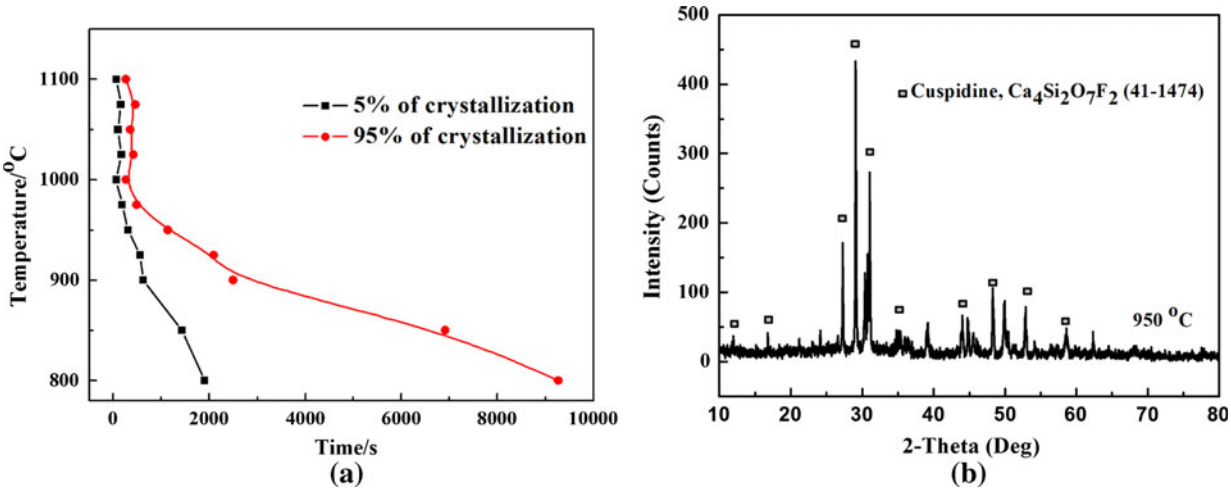

Fig. 13—TTT diagram of LC mold flux crystallization from glassy to crystal: (*a*) TTT diagram and (*b*) XRD of crystal at 1223 K (950 °C).

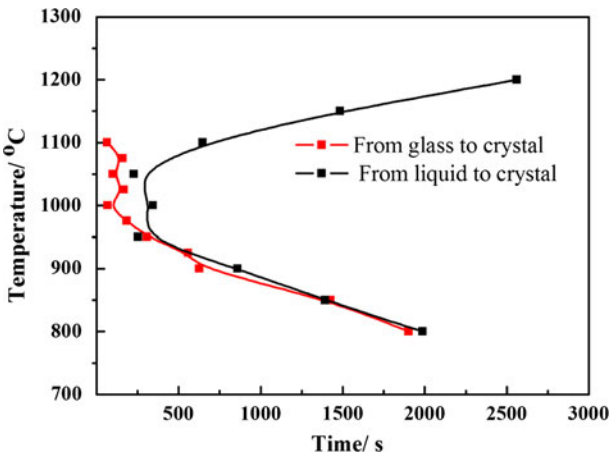

Fig. 14—The combined 5 pct of crystallization TTT diagrams of LC mold flux from glassy and liquid phases.

Figure 15 gives the TTT diagrams of MC mold flux crystallization from liquid phase and two typical crystal XRD results. The TTT curve of MC mold flux crystallization from liquid was double noses, which was different from the LC mold flux. The nasal tips were 1473 K (1200 °C) and 1623 K (1350 °C). It could be known that the MC mold flux was much easier to get crystallized. So the whole DHTT simulation experiment of MC mold flux was shorter than LC mold flux. The cooling rate of 30 °C/s red line intersects with the 5 pct of crystallization curve in Figure 15 (a), which explains why the liquid MC mold flux transformed directly into crystalline phase during the cooling process of the CH-2 in the DHTT experiment as shown in Figure 8(b). In fact, the rapid crystallization of mold flux at meniscus region can result in a moderate cooling of solidified shell in continuous casting of MC steels.[29,30]

X-ray diffraction analysis showed that the crystal phases of MC mold flux at lower temperature zone were cuspidine ($Ca_4Si_2O_7F_2$), but gehlenite ($Ca_2Al_2SiO_7$) precipitated at higher temperature zone in Figure 15, where $Ca_4Si_2O_7F_2$ was still found in the crystalline phase as an intermediate zone linking the two phases of high and low temperature.[7,31] These were consistent with the EDS results of Figures 11(b) and (c), where the

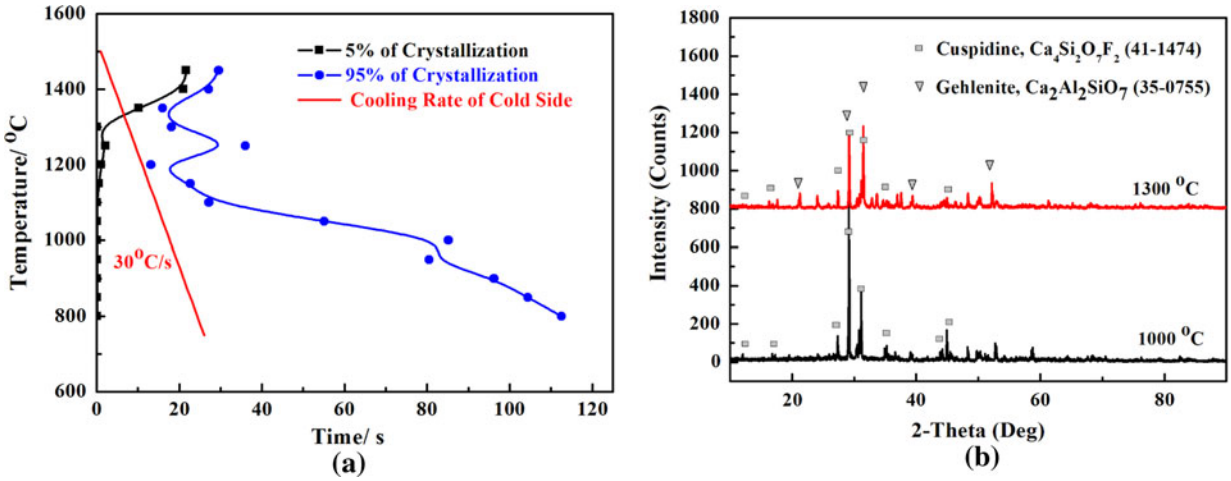

Fig. 15—TTT diagram of MC mold flux from liquid to crystal: (*a*) TTT diagram, (*b*) XRD of crystal at 1273 K (1000 °C), and 1573 K (1300 °C).

cuspidine was mainly formed in the low-temperature zone (crystal 3) and the gehlenite was precipitated in the high-temperature zone (crystal 4).

IV. CONCLUSIONS

The crystallization processes of LC and MC mold fluxes under the thermal conditions in continuous casting mold were *in situ* observed and investigated by using DHTT. The main conclusions were summarized as follows:

1. In the process of LC mold flux crystallization, the glass phase was first formed when the CH-2 was cooled to 1073 K (800 °C) with a cooling rate of 30 °C/s. Then, the fine crystal particles were precipitated at the liquid/glass interface and grew toward the glass. The dendritic crystals were later formed in the middle of the liquid mold flux and grew toward the hot side. The SEM and EDS resulted showed that both crystals formed from glass or liquid phase were dendrites and mainly $Ca_4Si_2O_7F_2$, but the size of crystals from liquid were larger than those from glass.
2. However, during the process of MC mold flux crystallization, the crystals were formed directly at the area close to CH-2 thermocouple, when the CH-2 temperature was dropped to 1073 K (800 °C) with a cooling rate of 30 °C/s. Then crystals began to precipitate in side with the hot liquid and grow to the middle. The growth velocity of MC flux crystals was faster than that of LC flux. The SEM and EDS results showed that the previously precipitated crystals were large dendrites, whereas the later ones were mainly equiaxed. The main composition of the earlier crystals was $Ca_4Si_2O_7F_2$, and $Ca_2Al_2SiO_7$ was formed laterally in the hot side.
3. The results obtained from DHTT experiments could be explained and supported by TTT diagrams of LC and MC mold fluxes. Both DHTT simulations and TTT diagrams could provide a powerful tool for the understanding of mold flux crystallization behavior in real continuous-casting mold.

ACKNOWLEDGMENTS

The work was supported by International Science & Technology Cooperation Program of China (2011DFA71390), New Century Excellent Talents Program Award (Chinese Ministry of Education, NCET-10-0797), and the Fundamental Research Funds for the Central Universities (2011JQ010).

REFERENCES

1. K.C. Mills, A.B. Fox, Z. Li, and R.P. Thackray: *Ironmaking Steelmaking*, 2005, vol. 32 (1), pp. 26–34.
2. L. Zhou, W. Wang, F. Ma, J. Li, J. Wei, H. Matsuura, and F. Tsukihashi: *Metall. Mater. Trans. B*, 2011, in press.
3. H. Nakada and K. Nagata: *ISIJ Int.*, 2006, vol. 46 (3), pp. 441–49.
4. R.G. Hill, N.D. Costa, and R.V. Law: *J. Non-Cryst. Solids*, 2005, vol. 351 (1), pp. 69–74.
5. Y. Kashiwaya, C.E. Cicutti, A.W. Cramb, and K. Ishii: *ISIJ Int.*, 1998, vol. 38 (4), pp. 348–56.
6. A.W. Cramb: *Report: American Iron and Steel Institute, Technology Roadmap Program*, Pittsburgh, PA, 2003.
7. G. Wen, H. Liu, and P. Tang: *J. Iron Steel Res. Int.*, 2008, vol. 15 (4), pp. 32–37.
8. J.W. Cho and S. Kim: *J. Kor. Inst. Metall. Mater.*, 2004, vol. 42 (3), pp. 302–03.
9. W. Wang, K. Gu, L. Zhou, and F. Ma: *ISIJ Int.*, 2011, vol. 51 (11), pp. 1838–46.
10. J.W. Cho and H. Shibata: *J. Non-Cryst. Solids*, 2001, vol. 282 (1), pp. 110–17.
11. H. Mizuno, H. Esaka, K. Shinozuka, and M. Tamura: *ISIJ Int.*, 2008, vol. 48 (3), pp. 277–85.
12. M. Campforts, K. Verscheure, and F. Verheghe: *Sohn International Symposium- Advanced Processing of Metals and Materials*, San Diego, CA, 2006, pp. 309–21.
13. H.G. Ryu, Z.T. Zhang, J.W. Cho, G.H. Wen, and S. Sridhar: *ISIJ Int.*, 2010, vol. 50 (8), pp. 1142–50.
14. W. Wang, L. Zhou, and K. Gu: *Metall. Mater. Int.*, 2010, vol. 16 (6), pp. 913–20.
15. Z. Li, R. Thackray, and K.C. Mills: *J. S. Afr. Inst. Min. Metall.*, 2004, pp. 813–29.
16. Y. Meng and B.G. Thomas: *Metall. Mater. Trans. B*, 2003, vol. 34B, pp. 707–25.

17. W. Wang: Ph.D. Dissertation, Carnegie-Mellon University, Pittsburgh, PA, 2007.
18. B. Coates and S.A. Argyropoulos: *Metall. Mater. Trans. B*, 2007, vol. 38B, pp. 243–55.
19. P.E. Ramirez-Lopez, P.D. Lee, K.C. Mills, and B. Santillana: *ISIJ Int.*, 2010, vol. 50 (12), pp. 1797–804.
20. P.E. Ramirez-Lopez, P.D. Lee, and K.C. Mills: *ISIJ Int.*, 2010, vol. 50 (3), pp. 425–34.
21. Y. Meng and B.G. Thomas: *Metall. Mater. Trans. B*, 2003, vol. 34B, pp. 685–705.
22. D.T. Stone and B.G. Thomas: *Can. Metall. Q.*, 1999, vol. 38 (5), pp. 363–75.
23. J. Cho, H. Shibata, T. Emi, and M. Suzuki: *ISIJ Int.*, 1998, vol. 38 (5), pp. 440–46.
24. J. Cho, H. Shibata, T. Emi, and M. Suzuki: *ISIJ Int.*, 1998, vol. 38 (3), pp. 268–75.
25. C. Orrling, S. Sridhar, and A.W. Cramb: *High temp. Mater. Proc.*, 2001, vol. 20 (3), pp. 195–200.
26. K.C. Mills, A.B. Fox, P.P. Thackray, and Z. Li: *VII International Conference on Molten Slags Fluxes and Salts*, The South African Institute of Mining and Metallurgy, Johannesburg, South Africa, 2004, pp. 713–21.
27. W. Wang, K. Blazek, and A. Cramb: *Metall. Mater. Trans. B*, 2008, vol. 39B, pp. 66–74.
28. A.J Moore, R.J. Phillips, and T.R. Gibbs: *Steelmaking Conf. Proc.*, 1991, pp. 615–21.
29. M. Kawamoto, Y. Tsukaguchi, N. Nishida, T. Kanazawa, and S. Hiraki: *ISIJ Int.*, 1997, vol. 37 (2), pp. 134–39.
30. A. Yamauchi, K. Sorimachi, T. Sakuraya, and T. Fujll: *ISIJ Int.*, 1993, vol. 33 (1), pp. 140–47.
31. C. Zhao, S. Junc, Y. Kashiwaya, H. Gaye, and H. Lee: *ISIJ Int.*, 2008, vol. 48 (6), pp. 747–54.